Predicting the Particle Size Distribution in Twin Screw Granulation through Acoustic Emissions

H.A. Abdulhussain[a], M.R. Thompson[a,*]

[a]*CAPPA-D/MMRI, Department of Chemical Engineering,*

McMaster University, Hamilton, Ontario, Canada

[*] Author to whom correspondence should be addressed.

Tel: (905) 525-9140 x 23213

mthomps@mcmaster.ca

Keywords: Acoustic Emission, Process analytical technology, Twin screw granulation, Impact mechanics, Artificial neural network

ABSTRACT

A non-destructive process analytical technology for monitoring the complex particle size distributions inherent to twin-screw granulation (TSG) was presented, based on ultrasonic acoustic emissions (AE). AE spectra were collected by discrete signal acquisition during the continuous impacts of granules on an inclined plate positioned below the exit of an extruder. The paper outlines the setup considerations associated with the impact plate, based on an examination of its location, thickness (0.7, 1.0, 1.5 mm) and angle of inclination (10-60°) and the resulting particle behavior at the plate, as determined by high-speed image analysis and AE monitoring. Subsequently, AE spectra were collected during the wet granulation of lactose monohydrate at different liquid-to-solid ratios from 8-14% and correlated with the particle size distributions (PSD) to train a neural network model. Predicted PSD for particle sizes from 400 to 7000 μm based on the AE spectra of validation trials showed the largest root mean squared error (RMSE) of 4.25 wt% at 2230 μm. After transforming the AE data with a newly created digital filter based on particle impact mechanics to address auditory masking, the error for predicting fractions of each particle size was significantly reduced to below 1 wt%. The technology shows great promise as a monitoring method for TSG, being capable of predicting its complex size distributions in real time.

Keywords: Acoustic Emission, Process analytical technology, Twin screw granulation, Impact mechanics, Artificial neural network

1. INTRODUCTION

The concept of continuous manufacturing has been gaining momentum in the pharmaceutical industry over the past two decades. The publications of the United States Food and Drug Administration (FDA) on process analytical technologies (PAT) along with the harmonized tripartite Q8 guideline of the International Council for Harmonization (ICH) of 'Technical Requirements for Pharmaceuticals for Human Use' paved the way for regulatory acceptance of novel manufacturing technologies to be used in the production of solid oral dosage forms[1,2]. The advantages of continuous, in comparison to batch, manufacturing for drug products rely upon its higher product consistency, reduced costs associated with product scale-up, and ability to readily implement PAT[2,3].

Twin screw granulation (TSG) has gained much attention over the past decade as a continuous manufacturing technology for wet, foam, heat-assisted and hot melt granulation[3–5]. The advantages of TSG over other manufacturing technologies are its closely confined mixing characteristics, short residence time (seconds compared to minutes or hours), and modular process configuration, which dramatically reduce its equipment footprint[6,7]. One key difference between TSG and its batch counterpart is the particle size distribution (PSD) produced. A batch granulation process is expected to produce a unimodal (Gaussian) distribution whereas TSG typically produces a bimodal distribution for the same formulation[6,8–10]. The PSD is vital to determining tablet properties, such as strength and porosity, which ultimately affect the rate that this type of dosage form disintegrates upon ingestion[11,12].

From a monitoring perspective, the challenges associated with a bimodal distribution are unique, since simple numerical descriptors such as the mean particle size or the span of the distribution have little correlated meaning with tabletting, unlike for a Gaussian distribution. This presents a unique need for PAT within TSG to show correlation with the PSD, not just simple particle size descriptors, to monitor for quality consistency. PAT currently examined for in-line granulation monitoring include near infrared (NIR) spectroscopy[13,14] and image processing[11,14,15], though the latter is more prevalent industrially for particle sizing at the moment. Both of these approaches have the advantage of being non-destructive and can be integrated directly into the manufacturing process[13,14]. However, NIR spectroscopy requires a large amount of data for calibration and it is subject to sensor fouling which can lead to spurious results[16]. Image processing (ex. the commercial Horiba Eyecon™ system) is also subject to fouling/dust accumulation around its optics and exhibits resolution issues when looking at extremes in particle sizes[17,18]. Both are good non-destructive technologies with no risk of interfering with or contaminating the granulation process but a more robust approach that was immune to fouling would be advantageous if it could address the aforementioned complexities of the PSD for TSG. Other potential techniques such as laser diffraction, mechanical vibrations, and electrostatic sensing have been shown to be feasible to predict particle size but are difficult to implement in a manufacturing setting due to their high costs, lower perceived sensor durability, accuracy, and reliability [19–21].

Acoustic Emissions (AE) is an approach not yet considered for TSG monitoring but conceivably well suited to the process based on its advantages of needing no calibrations, greater immunity to the influences of fouling/dust accumulation, and low implementation costs[22]. It would not be a completely novel approach since AE has been used for monitoring in the past of other particulate process operations, both within[23–26] and outside[27–29] of the pharmaceutical industry. The associated technique relate features of a detected signal to the particle impacts or collisions that generated these acoustic emissions. Most notable examples have been reported for high shear batch granulation, in order to determine the endpoint of the process and to predict a Gaussian particle size distribution [26,30]. Outside the pharmaceutical industry, multiple studies have involved pneumatic conveyers, fluidized beds, and milling units, using AE analysis to once again predict a Gaussian distribution[19–22,29]. Approaches for applying AE to monitor much more complex particle size distributions have yet to be disclosed in the literature.

In this regard, the present study investigates the means for developing a robust non-destructive PAT capable of monitoring the complex PSD produced by continuous granulation via TSG. To predict weight fractions for a broad range of anticipated granule sizes, it is postulated that the intensity of a set of frequencies in an acquired AE spectrum can be correlated to the impact mechanics of specific particle sizes. Furthermore, it is postulated that with appropriate signal processing and selection of a neural network model that bimodal PSD may be predicted in real-time for this continuous process.

2. MATERIALS AND METHODS

2.1. Materials and Process Setup

Granulation was completed in a 27 mm 40 L/D Model ZSE-27HP corotating twin screw extruder (Leistritz Extrusion; Somerville, NJ, USA). The barrel consisted of a water-cooled feed zone (Z0) and nine barrel zones (Z1–Z9) actively controlled at 35°C. The screw speed for all experiments was 200 RPM. Flowlac® 100 α-lactose monohydrate (Meggle Pharma; Wasserburg, Germany) was chosen as the placebo formulation for the study due to its low water solubility, minimizing the effects of moisture on the acoustics during this preliminary stage of PAT development. The lactose was introduced into the extruder at a constant flow rate of 4 kg/h for all experiments using a Brabender T20 twin-screw gravimetric feeder (Mississauga, ON, Canada). An aqueous solution of 4 wt% METHOCEL™ E3PLV (DuPont Nutrition & Biosciences;

Midland, MI, USA) was used as the liquid binder in this work and injected into the extruder at zone Z2 using an ISCO 260D high pressure syringe pump (Teledyne-ISCO Inc.; Lincoln, NE, USA) at varying liquid-to-solids (L/S) ratios of 8, 10, 12, 13, and 14%[31,32]. The liquid was injected in the intermeshing region between the two screws. Experiments for each L/S ratio were repeated 10 times to build a sizeable dataset for the modeling technique described in a later section. The screw design employed for these experiments consisted of multiple conveying elements with pitches of 30 and 20 mm from Z1-Z7 followed by two kneading blocks with discs at 60 degrees offset in Z8 and then subsequent conveying elements in Z9; the screw design is typical for twin-screw wet granulation.

2.2.Particle Size Analysis

The granules produced from the extruder were air-dried at room temperature for 48 hours to below 5 % (w/w) moisture content before being analyzed for their size; moisture content was determined using an HG63 moisture analyzer (Mettler-Toledo; Columbus, OH). PSD data was determined using a Ro-Tap RX-29 sieve shaker (W.S. Tyler; Mentor, OH, USA). A granulated sample of 100 g for each L/S ratio was originally classified into eight size fractions (using sieves of 2100, 1700, 1400, 1180, 850, 500, and 300 μm nominal openings, as well as the bottom pan) by mechanically agitating for five minutes. The weight difference before and after sieving was used to find the wt% for each bin in the distribution. The mass on the 2100 μm sieve was subsequently classified further by reconfiguring the shaker with sieves of 8000, 6300, 4760, 3350, 2360, 2100, and 1700 μm nominal openings and mechanically agitating for another five minutes. Similarly, the mass in the bottom pan from the original agitation was subsequently classified further by reconfiguring the shaker with sieves of 500, 300, 250, 180, 150, 53, and 44 μm nominal opening and once more, mechanically agitating for five minutes. During the TSG experiments, granule sizes changed from very fine to very coarse, much more broadly than normal granulation operations. The sieving of the granules on the 2100 μm sieve and pan was done in order to capture all possible changes across different L/S ratios for the neural network model implemented in the subsequent section.

2.3. Acoustic Signal Acquisition

To record the continuous particle impacts exiting from the extruder, a F15α broadband sensor that was most sensitive to frequencies between 100 to 450 kHz (Physical Acoustics; Princeton, NJ, USA) was attached to a 25.4 mm x 25.4 mm tab that extended from a SAE 304 stainless steel (SS) impact plate with dimensions of 44.5 mm x 76.2 mm; seating the sensor on the tab, off to the side of the plate, was preferred since the envisioned PAT design positions the plate inside the exit chute of a TSG but ready access to the sensor will demand that it be positioned outside of the chute walls. The sensor was fitted to the impact plate using high vacuum grease (Dow Corning) to improve contact. Figure 1 shows the sensor and impact plate assembly.

The detected signal with the sensor was amplified using a Physical Acoustics 2/4/6c amplifier set to +60 dB and collected using a National Instruments 3.5 MHz 12-bit 4-channel data acquisition system. For each experiment, 30 seconds of data was collected from the collisions of granules onto the plate at a sampling rate of 3 MHz. The vertical distance of the plate relative to the exit of the extruder was based on an analysis of apparent terminal velocity to ensure consistency of the impacts. Approximately 97% of the particles for Flowlac® 100 were below 250 μm [33] and so, the smallest particle chosen to be a 'granule' in the model was 300 μm based on the minimum sieve size in the study unlikely to capture ungranulated solids. The drop distance for a 300 μm particle to reach terminal velocity was found to be roughly 20 cm below the exit of the extruder, which is where the plate was positioned. This was done for all experiments mentioned below. The terminal velocity analysis was done to ensure the impacts of particles at the top or bottom of the plate would be relatively consistent with one another. Figure 2 shows a schematic for the experimental setup with the extruder and impact plate assembly.

2.4. Studies of Plate Angle and Plate Thickness

Initially, the impact plate setup was examined for differing inclinations of 10, 30, 45, and 60 degrees relative to the horizontal plane with a fixed plate thickness of 0.7 mm. Only granulation at 8% L/S ratio was tested in this case. AE sampling for a 30 s duration was repeated three times, for every angle to account for statistical and acoustic variance. The trajectory and mechanical integrity of granules colliding with the plate was observed at a distance of 10 mm away from the edge of the plate by high speed image analysis taken using a FASTCAM SA-Z type 2100k camera (Photron Limited, Tokyo, Japan) operating at 20,000 frames per second. Analysis of videos was done using Photron FastCam Viewer 4 software.

In the second stage of experiments analyzing the impact plate setup, granule collisions were recorded for 30 s for plates with thicknesses of 0.7, 1, and 1.5 mm at a fixed inclination of 60°. In this case, more extensive granulation was performed at 8, 10, 12, 13, and 14% L/S ratios for each plate thickness. The AE sampling for 30 s was repeated three times for every L/S ratio to account for statistical and acoustic variance.

2.5. Granulation Experiments for Model Training and Validation

AE monitoring of particle collisions on the 1.5 mm thick impact plate angled at 60 degrees inclination relative to the horizontal plane, were recorded according to Sec 2.3. TSG trials were performed at L/S ratios of 8, 10, 12, 13, and 14%. At 8% it was found there was a large amount of ungranulated particles whereas 14% was found to be the maximum saturation before the granules turned into sludge. This range ensured AE spectra was collected from very fine to very coarse granules. AE sampling for 30 s was repeated ten times per L/S ratio to generate a large training dataset for modeling and to account for statistical and acoustic variance.

With an estimated flowrate of 1.1 g/s, a sampled signal of 30 s duration corresponded to thousands or tens of thousands of collisions depending on the selected operating conditions with the extruder. Factoring in repeats, more than 4,800 sampled signals were recorded for the training and validation experiments. A discrete Haar wavelet filter was used to reduce noise followed by Fast Fourier Transform (FFT) to view each processed signal in the frequency domain. With no visible peaks roughly above 600 kHz, the chosen frequency range of analysis was 0-700 kHz in this study. Each signal dataset was reduced in size for the model, decreasing the frequency resolution from 3 Hz to 67 Hz.

A granular sample of roughly 300 g was collected for each L/S ratio after the 10 sampled signals were collected. The PSD for the trial was determined by analyzing 100 g of the collected granules. Three repeats were done to assess the error in the sieving measurement. Following the characterization method in Sec 2.2, weight fractions were determined for the corresponding average particle sizes (>8000, 7150, 5530, 4055, 2855, 2230, 1900, 1550, 1290, 1015, 675, 400, 275, 215, 165, 102, 49, and <44 μm). Weight fractions above 7150 μm and below 49 μm were zero wt%, and did not change as the L/S ratio increased. As a result, the size fractions of >8000 and <44 μm were not included in the final dataset to reduce redundancies, making the final distribution composed of 16 weight fractions in the model.

2.6. Designing an AE Impact Filter

A particle monitoring system based on impacts, where granules spanning a wide range of sizes (and strengths) presents a challenge known as auditory or spectral masking. The “sound” produced by a large particle impacting a plate will overshadow the sound produced by a smaller particle colliding at the same time or closely thereafter. Since the principle of an acoustic monitoring method is to relate the amplitude of a signal (or specific frequencies in the signal) to a count of particles, masking may have a detrimental effect on the predicted PSD. To address this issue, a digital signal filter was conceived to alleviate auditory masking at the impact plate, derived from Hertz theory for single particle impacts.

The work by Rao describes the transverse response, normal modes, along with the force response when an impact force is applied to a metal plate at rest [34]. They are shown in Equations (1), (2), (6), and (7) below. The transverse response of the plate shown in Equation (1) below is a function of both the normal modes of the plate along with the plate response to the force applied.

$$w(x, y, t) = \sum_{m=1}^{\infty} \sum_{n=1}^{\infty} W_{mn}(x, y) \eta_{mn}(t) \tag{1}$$

where W_{mn} represents the normal modes of the plate and η_{mn} is the plate response to the force applied. M and n correspond to the modal numbers for the x and y direction. The normal modes are of the plate are:

$$W_{mn} = \frac{2}{\sqrt{\rho h a b}} \sin\left(\frac{m\pi x}{a}\right) \sin\left(\frac{n\pi y}{b}\right) \tag{2}$$

where ρ, h, a, b are the density, thickness, length, and width of the plate, respectively. Assuming the particles are spherical and collisions are elastic, the force can be modelled with the Hertz theory of impact as shown [35,36]:

$$F(t) = F_0 \sin\left(\frac{\pi t}{t_c}\right) = F_0 \sin(\pi \Omega \mathrm{t}) \tag{3}$$

with F_0 being the maximum force and t_c being the contact time of a collision, and Ω is the frequency of the impact force. Expressions for the maximum force and contact time are given in Equations (4) and (5), respectively:

$$F_0 = 1.917\rho_1^{\frac{3}{5}}\left(\frac{1-v_1}{\pi E_1}+\frac{1-v_2}{\pi E_2}\right)^{-2/5} R^2 V_0^{6/5} \tag{4}$$

$$t_c = 4.53\left(\frac{4\rho_1\pi\left(\frac{1-v_1}{\pi E_1}+\frac{1-v_2}{\pi E_2}\right)}{3}\right)^{2/5} R V_0^{6/5} \tag{5}$$

where ρ_1 is the density of the particle, v_1 and E_1 refer to the Poisson ratio and Young's Modulus of lactose monohydrate. R is the particle radius and V_0 is its impact velocity. Knowing the impact force, the response of the plate to the force can be determined and is shown as:

$$\eta_{mn}(t) = \frac{2F_0}{(\omega_{mn}^2-\Omega^2)\sqrt{\rho hab}}\sin\left(\frac{m\pi x_0}{a}\right)\sin\left(\frac{n\pi y_0}{b}\right)(\omega_{mn}\sin\Omega \mathrm{t} - \Omega\sin\omega_{mn}t) \tag{6}$$

where x_0 and y_0 are the points of impact on the plate, and ω_{mn} is the natural frequency of the plate:

$$\omega_{mn} = \pi^2\left[\left(\frac{m}{a}\right)^2+\left(\frac{n}{b}\right)^2\right]\sqrt{\frac{E_2h^3}{12(1-v_2)\rho h}} \tag{7}$$

where E_2 and v_2 are the Young's Modulus and the Poisson's ratio for the plate, respectively. The plate compression for a single particle dropping onto a plate was then computed from Equation (1). The parameters used in Equations (1) – (7) are shown in Table 1.

Figure 3 (a) shows the plate response, on a frequency basis, for the impact of a 100 μm particle. The plate response of a single granule of 49 to 7150 μm size impacting a stainless steel plate at its epicenter, on a frequency basis, is shown in Figure 3 (b). As particle size increases, the plate is seen to vibrate at a lower frequency, giving an inverse relationship. This trend was also noted by others[37–39] and allows the user to understand and roughly correlate peaks in the spectrum with their particle size.

Assuming granules impacting the plate are spherical in nature, the mass of a single granule is calculated per particle size (49 – 7150 μm). It is assumed that the maximum mass of any particle that will strike the plate is equal to the flowrate in g/s over a one second basis (1.1 g in this study). The maximum mass is divided by the mass of every particle to obtain an approximate number of granules per particle size. The theoretical amplitude for each particle size is then scaled by the number of granules for its respective size. The measured amplitude from the AE experiments is then divided by the maximum amplitude at the theoretical impact frequency found in Figure 3 (c) to filter for auditory masking and produce the final spectrum.

2.7. Neural Network Model

To relate the data-intensive impact acoustic signal to particle sizes, an artificial neural network (ANN) model was employed due to the exhibited nonlinearity in the modelled environment. These types of models have been shown to be superior to statistical modeling when looking at highly non-linear systems[40–42], making them attractive for the purposes of predicting PSD from an AE signal. Before modeling, stratified splitting was used to ensure the training and testing sets contained an equal proportion of data for each L/S ratio. Each L/S ratio dataset was split into 80% training and 20% testing. Then 10% of the training data was used for validation during model training. Principal component analysis (PCA) was used on the training set to reduce the dataset dimensions down to 12 components which contain 64.5% of the variance in the original data. Both PCA and the ANN were setup in Python using the *sklearn* library.

For the case of the testing set, the acoustic signal from granule collisions for each L/S ratio were averaged in the testing set giving one representative spectrum for each L/S ratio. This strategy allows for simplicity when performing new experiments as well as gives the opportunity to see the prediction error for each distribution. When predicting PSD with the testing set, loadings from a PCA model were used to convert the dataset into scores. The scores are then fed into the ANN to predict the PSD. The ANN employed an input layer with 12 nodes, which correspond to the number of components from PCA. This was followed by 3 hidden layers at 500 nodes, 250, and 100 nodes, respectively along with one output layer with 16 nodes, corresponding to each particle size. The Rectified Linear Unit activation function (ReLU) was used for the input and first hidden layer. The second and third hidden layers had the hyperbolic tangent (tanh) and sigmoid function, respectively, while the output layer had a linear activation function. 50% dropout regularization was employed between layers to minimize overfitting. The chosen Loss function was the mean squared error (MSE). To quantify prediction error in the model, the root mean squared error (RMSE) was used.

For the case when the model used the AE Impact Filter, the training, testing, and validation datasets were identical to the original approach. In this case, PCA was not used to compress the AE data since it was found to worsen predictions when the filter was used. The ANN architecture was identical to the case without the filter, both in terms of the activation functions and number of layers. The only difference being the input layer had 10395 nodes due to PCA not being used to reduce the dataset.

3. RESULTS AND DISCUSSION

3.1. Effect of Impact Plate Angle

Exiting granules from the extruder were targeted to collide at the epicenter of the plate to optimally minimize both plate vibrations and AE signal attenuation. The incline angle of the impact plate will have a strong influence on the amplitude of acoustic emissions due to the contact mechanics present. Figure 4 plots the average maximum amplitude in the spectra collected for inclined plate angles of 10, 30, 45, and 60 degrees relative to the horizontal plane. The maximum amplitude was seen to increase as the incline angle increased until 45 degrees, reflecting the gain in AE signal intensity associated with particle impacts. This seems contrary to expectation, at least following the theory of single particle impacts which anticipates the amplitude of AE associated with a collision should be greater for smaller inclinations [39]. The trend seen for amplitude was attributed to the accumulated mass observed on the plate over time at angles of 10 and 30 degrees, dampening the impact force of subsequent colliding particles. Conditions at 45 and 60 degrees showed no accumulated mass on the plate but as expected, the amplitude decreased for the steeper angle in these two cases due to decreasing normal collision forces by falling particles.

Based on the trend in maximum amplitude, it might be naturally assumed that the choice for plate inclination in the setup would have been at 45 degrees; however, the effects of granular breakage and secondary collisions on the spectra must also be considered. Figure 5 shows the captured motion of granules colliding with the impact plate at 45 and 60 degrees inclination, as observed by high speed image analysis. At 45 degrees, more granular damage was observed during the primary collision with the plate and rebounding particles had a greater chance of striking the plate again. At 60 degrees, the decreased normal force reduced the damage seen by granules as they collided with the plate and since they departed the field of view by ‘sliding or rolling’, there was little likelihood of a detectable secondary impact. Despite the lower signal amplitude at 60 degrees, this condition was chosen as the preferred plate incline angle.

It is expected that some granule breakage will always occur regardless of the inclination angle of the plate. Such breakage has more influence on a rebounding rather than an impacting particle and hence, more significantly affect the PSD rather than acoustic emission in our study. Fortunately, the absence of detectable breakage in the captured video of impacts at 60 degrees inclination gave increased confidence that the signal was being correlated to an accurate representation of the particles that produced the acoustic emissions.

3.2. Effect of Impact Plate Thickness

The other setup parameter studied was plate thickness. Figure 6 shows AE spectra for plates of different thicknesses, constantly inclined at 60 degrees to the horizontal plane. There was generally no change in the nature of the spectra for the same L/S ratio as the thickness increased from 0.7 to 1.5mm; however, the signal amplitude decreased as the thickness of the plate increased, most notably seen for the spectra at 13 and 14% L/S ratios. Particle impacts onto the 0.7 mm plate were creating detectable vibrations in the plate itself during experiments implying particles might contact onto the plate multiple times during a single collision event due to the rebound motion of the plate, thereby increasing the measured amplitude. As its thickness increased the plate vibrated less from the particle impacts. A thickness of 1.5 mm was considered acceptable for the final setup since no motion from the plate was observed during experiments, and yet the signal strength was sufficient for the model to distinguish different particle collisions.

3.3. Signal Analysis based on Particle Size

Figure 7 shows the average acoustic spectra from the TSG experiments for each L/S ratio along with their respective PSDs. The observable trend in AE spectra, shown in Figure 7(a), was a decrease in the amplitude as L/S ratio increased, with the main regions of interest being 50-150 kHz and 200-300 kHz. From plate response calculations in Figure 3(b), the 50-150 kHz region corresponds to 300 – 1000 μm particle impacts and the 200-300 kHz region relates to 150 – 240 μm particle impacts. Correspondingly, Figure 7(b) shows that as the L/S ratio increased, the weight fraction of granules between 49 – 1550 μm decreased substantially, seeming to corroborate the decrease in amplitude in the AE spectra. While the plate response frequency assignments were derived only for single particle impacts, they appear to be suitably correlated with the particle sizes under this study from TSG. Impacts of particles above 2200 μm in size were predicted to produce plate responses around 20-50 kHz, beyond the ideal sensitivity range of the broadband sensor. AE associated with these larger particles still exhibited detected frequencies (harmonics) in the experiments that could be discriminated by the model but the current setup should be considered reasonable for monitoring particles below 3000 μm. Since the largest granule size suitable for tableting is 1.25 mm[43–45], the current setup was considered suitable for the purposes of introducing the ANN model. Future studies will consider the advantages of a two sensor system to acquire a broader range of frequencies so that the model might have a better capacity to predict very coarse granules via TSG.

3.4. Model Training and Validation

Confidence in the model predictions was evaluated based on RMSE calculated for the testing AE spectra corresponding to granulation at each L/S ratio, as shown in Figure 8. Predicted PSDs based on the testing datasets processed without and with the impact filter are shown in Figure 9 and 10, respectively along with their experimentally measured PSD for each L/S ratio. For the case of processing the AE data without the impact filter, the RMSE for the majority of particle sizes was below 2 wt% for all L/S ratios. This is reflected in Figure 9 where the model was able to fit each PSD fairly well. The particle size with the highest error was 2230 μm for PSD at 12% L/S ratio, which goes up to 4.25 wt% RMSE as seen in Figure 8 (a). This high RMSE is attributed to the PSD being strongly bimodal with both peaks being nearly equal to one another, which likely increased the difficulty in predictions. In general, the model without the filter was considered to have satisfactorily learned to associate the AE spectra to sets of particles colliding with the impact plate, at least for the specific case of lactose monohydrate which granulates at much lower degrees of saturation than most pharmaceutical formulations. Future studies will be required to understand how formulations and degree of saturation affect the AE spectra and the model's ability to associate acoustics to particle size. This will enable the prediction error for each particle size to be tracked for different formulations making this potentially a very powerful monitoring tool when producing multiple products from the same TSG.

For the case of processing the AE spectral data with the impact filter, a significant decrease was seen in the prediction error in comparison to Figure 8(a), now at or below 1 wt% RMSE for all particle sizes being considered. This improved accuracy in predicted PSD is reflected in Figure 10 where the model and experimental sieved weight fractions are much closer in value. With the impact filter, the loss error was no longer localized around 2230 μm, highlighting the effect that auditory masking was having on the AE signal in the original model. Diminishing auditory masking of the signal allowed the model to more equally consider the contribution of all frequencies (and particle collisions) in the response.

4. CONCLUSION

Ultrasonic acoustic emissions were explored as an approach for PAT to monitor the exiting particle size from a twin screw granulator, a continuous granulation method noted for producing complex size distributions. The elements of the approach consisted of a 1.5 mm thick stainless steel impact plate, ideally inclined at 60 degrees to minimize powder accumulation and ensure rebounding trajectories did not allow for secondary collisions by granules from the granulator. Using an artificial neural network model and PCA to reduce the dimensions of the dataset, error analysis showed the model experienced the most difficulty predicting the distribution when it was strongly bimodal, with the highest reported error of 4.25 wt% for the 2230 μm fraction. Applying a newly introduced impact filter to the AE data to minimize auditory masking, the model error decreased significantly below 1 wt% and became evenly distributed amongst all particle sizes rather than being localized to the larger particles in the exiting distribution. For this preliminary study for an AE-based PAT approach, the training was done with lactose monohydrate, but future studies will follow to examine how formulation and level of saturation affects acoustic emissions of impacting granules. It is anticipated that plate design and the auditory masking filter will require revisions as fracture strength and cohesiveness change the nature of particle impacts. Practically speaking, the accuracy of the approach will also need study as the flow rate increases to production levels and only a fraction of the exiting mass is impacting the plate.

5. ACKNOWLEDGEMNTS

The authors would like to thank Kevin O' Donnell from Dupont Biosciences and Nutrition for providing the materials used in this study and the Natural Sciences and Engineering Research Council (NSERC) for funding the work. The authors would also like to thank Austin Bedrosian and Vladimir Gritsichine for their helpful insights in the early stages of data analysis.

6. REFERENCES

[1] M. Fonteyne, A. Correia, S. De Plecker, J. Vercruysse, I. Ilić, Q. Zhou, C. Vervaet, J.P. Remon, F. Onofre, V. Bulone, T. De Beer, Impact of microcrystalline cellulose material attributes: A case study on continuous twin screw granulation, Int. J. Pharm. 478 (2015) 705–717. https://doi.org/10.1016/j.ijpharm.2014.11.070.

[2] C. Portier, K. Pandelaere, U. Delaet, T. Vigh, A. Kumar, G. Di Pretoro, T. De Beer, C. Vervaet, V. Vanhoorne, Continuous twin screw granulation: Influence of process and formulation variables on granule quality attributes of model formulations, Int. J. Pharm. 576 (2020) 118981. https://doi.org/10.1016/j.ijpharm.2019.118981.

[3] E.I. Keleb, A. Vermeire, C. Vervaet, J.P. Remon, Twin screw granulation as a simple and efficient tool for continuous wet granulation, Int. J. Pharm. 273 (2004) 183–194. https://doi.org/10.1016/j.ijpharm.2004.01.001.

[4] B. Mu, M.R. Thompson, Examining the mechanics of granulation with a hot melt binder in a twin-screw extruder, Chem. Eng. Sci. 81 (2012) 46–56. https://doi.org/10.1016/j.ces.2012.06.057.

[5] K.E. Rocca, S. Weatherley, P.J. Sheskey, M.R. Thompson, Influence of filler selection on twin screw foam granulation, Drug Dev. Ind. Pharm. 41 (2015) 35–42. https://doi.org/10.3109/03639045.2013.845839.

[6] A. Ito, P. Kleinebudde, Influence of granulation temperature on particle size distribution of granules in twin-screw granulation (TSG), Pharm. Dev. Technol. 24 (2019) 874–882. https://doi.org/10.1080/10837450.2019.1615089.

[7] J. Vercruysse, A. Burggraeve, M. Fonteyne, P. Cappuyns, U. Delaet, I. Van Assche, T. De Beer, J.P. Remon, C. Vervaet, Impact of screw configuration on the particle size distribution of granules produced by twin screw granulation, Int. J. Pharm. 479 (2015) 171–180. https://doi.org/10.1016/j.ijpharm.2014.12.071.

[8] A.S. El Hagrasy, J.D. Litster, Granulation rate processes in the kneading elements of a twin screw granulator, AIChE J. 59 (2013) 4100–4115. https://doi.org/10.1002/aic.14180.

[9] R.M. Dhenge, K. Washino, J.J. Cartwright, M.J. Hounslow, A.D. Salman, Twin screw granulation using conveying screws: Effects of viscosity of granulation liquids and flow of powders, Powder Technol. 238 (2013) 77–90. https://doi.org/10.1016/j.powtec.2012.05.045.

[10] B. Van Melkebeke, C. Vervaet, J.P. Remon, Validation of a continuous granulation process using a twin-screw extruder, Int. J. Pharm. 356 (2008) 224–230. https://doi.org/10.1016/j.ijpharm.2008.01.012.

[11] B. Presles, Novel image analysis method for in situ monitoring the particle size distribution of batch crystallization processes, J. Electron. Imaging. 19 (2010) 031207. https://doi.org/10.1117/1.3462800.

[12] A.F.T. Silva, A. Burggraeve, Q. Denon, P. Van Der Meeren, N. Sandler, T. Van Den Kerkhof, M. Hellings, C. Vervaet, J.P. Remon, J.A. Lopes, T. De Beer, Particle sizing measurements in pharmaceutical applications: Comparison of in-process methods versus off-line methods, Eur. J. Pharm. Biopharm. 85 (2013) 1006–1018. https://doi.org/10.1016/j.ejpb.2013.03.032.

[13] T. De Beer, A. Burggraeve, M. Fonteyne, L. Saerens, J.P. Remon, C. Vervaet, Near

infrared and Raman spectroscopy for the in-process monitoring of pharmaceutical production processes, Int. J. Pharm. 417 (2011) 32–47. https://doi.org/10.1016/j.ijpharm.2010.12.012.

[14] J. Huang, C. Goolcharran, J. Utz, P. Hernandez-Abad, K. Ghosh, A. Nagi, A PAT approach to enhance process understanding of fluid bed granulation using in-line particle size characterization and multivariate analysis, J. Pharm. Innov. 5 (2010) 58–68. https://doi.org/10.1007/s12247-010-9079-x.

[15] C.R. Malwade, H. Qu, Process Analytical Technology for Crystallization of Active Pharmaceutical Ingredients, 2018. https://doi.org/10.2174/1381612824666180629111632.

[16] C. Buschmueller, W. Wiedey, C. Doescher, M. Plitzko, J. Breitkreutz, In-line Monitoring of Granule Moisture and Temperature throughout the entire Fluidized-bed Granulation Process using Microwave Resonance Technology Part I, Pharm. Ind. 71 (2009) 1403-+.

[17] P. Suresh, I. Sreedhar, R. Vaidhiswaran, A. Venugopal, A comprehensive review on process and engineering aspects of pharmaceutical wet granulation, Chem. Eng. J. 328 (2017) 785–815. https://doi.org/10.1016/j.cej.2017.07.091.

[18] A. Kumar, J. Dhondt, F. De Leersnyder, J. Vercruysse, V. Vanhoorne, C. Vervaet, J.P. Remon, K. V. Gernaey, T. De Beer, I. Nopens, Evaluation of an in-line particle imaging tool for monitoring twin-screw granulation performance, Powder Technol. 285 (2015) 80–87. https://doi.org/10.1016/j.powtec.2015.05.031.

[19] A. Bastari, C. Cristalli, R. Morlacchi, E. Pomponi, Acoustic emissions for particle sizing of powders through signal processing techniques, Mech. Syst. Signal Process. 25 (2011) 901–916. https://doi.org/10.1016/j.ymssp.2010.08.019.

[20] Y. Hu, X. Qian, X. Huang, L. Gao, Y. Yan, Online continuous measurement of the size distribution of pneumatically conveyed particles by acoustic emission methods, Flow Meas. Instrum. 40 (2014) 163–168. https://doi.org/10.1016/j.flowmeasinst.2014.07.002.

[21] A. Boschetto, F. Quadrini, Powder size measurement by acoustic emission, Meas. J. Int. Meas. Confed. 44 (2011) 290–297. https://doi.org/10.1016/j.measurement.2010.10.005.

[22] C.J. Ren, J.D. Wang, D. Song, B.B. Jiang, Z.W. Liao, Y.R. Yang, Determination of particle size distribution by multi-scale analysis of acoustic emission signals in gas-solid fluidized bed, J. Zhejiang Univ. Sci. A. 12 (2011) 260–267. https://doi.org/10.1631/jzus.A1000396.

[23] S. Matero, S. Poutiainen, J. Leskinen, K. Järvinen, J. Ketolainen, S.P. Reinikainen, M. Hakulinen, R. Lappalainen, A. Poso, The feasibility of using acoustic emissions for monitoring of fluidized bed granulation, Chemom. Intell. Lab. Syst. 97 (2009) 75–81. https://doi.org/10.1016/j.chemolab.2008.11.001.

[24] M. Whitaker, G.R. Baker, J. Westrup, P.A. Goulding, D.R. Rudd, R.M. Belchamber, M.P. Collins, Application of acoustic emission to the monitoring and end point determination of a high shear granulation process, Int. J. Pharm. 205 (2000) 79–91. https://doi.org/10.1016/S0378-5173(00)00479-8.

[25] M.J. Waring, M.H. Rubinstein, J.R. Howard, Acoustic emission of pharmaceutical materials during compression, Int. J. Pharm. 36 (1987) 29–36. https://doi.org/10.1016/0378-5173(87)90232-8.

[26] M.K. Papp, C.P. Pujara, R. Pinal, Monitoring of high-shear granulation using acoustic emission: Predicting granule properties, J. Pharm. Innov. 3 (2008) 113–122.

https://doi.org/10.1007/s12247-008-9030-6.

[27] Y. Hu, L. Wang, X. Huang, X. Qian, L. Gao, Y. Yan, On-line sizing of pneumatically conveyed particles through acoustic emission detection and signal analysis, IEEE Trans. Instrum. Meas. 64 (2015) 1100–1109. https://doi.org/10.1109/TIM.2014.2355653.

[28] C. Aldrich, D.A. Theron, Acoustic estimation of the particle size distributions of sulphide ores in a laboratory ball mill, J. South African Inst. Min. Metall. 100 (2000) 243–248.

[29] H.W. Shen, H.R. Hardy, A.W. Khair, Laboratory study of acoustic emission and particle size distribution during rotary cutting, Int. J. Rock Mech. Min. Sci. Geomech. Abstr. 34 (1997) 635–636. https://doi.org/10.1016/S1365-1609(97)00247-5.

[30] E.M. Hansuld, L. Briens, A. Sayani, J.A.B. McCann, An investigation of the relationship between acoustic emissions and particle size, Powder Technol. 219 (2012) 111–117. https://doi.org/10.1016/j.powtec.2011.12.025.

[31] E.I. Keleb, A. Vermeire, C. Vervaet, J.P. Remon, Continuous twin screw extrusion for the wet granulation of lactose, Int. J. Pharm. 239 (2002) 69–80. https://doi.org/10.1016/S0378-5173(02)00052-2.

[32] M.R. Thompson, J. Sun, Wet granulation in a twin-screw extruder: Implications of screw design, J. Pharm. Sci. 99 (2010) 2090–2103. https://doi.org/10.1002/jps.21973.

[33] FlowLac® Product Detail - Meggle Pharma - Excipients & Technology, (n.d.). https://www.meggle-pharma.com/en/lactose/10-flowlac-100.html.

[34] S.S. Rao, Vibration of Continuous Systems, 2007. https://doi.org/10.1002/9780470117866.

[35] G.C. McLaskey, S.D. Glaser, Hertzian impact: Experimental study of the force pulse and resulting stress waves, J. Acoust. Soc. Am. 128 (2010) 1087. https://doi.org/10.1121/1.3466847.

[36] J. Reed, Energy losses due to elastic wave propagation during an elastic impact, J. Phys. D. Appl. Phys. 18 (1985) 2329–2337. https://doi.org/10.1088/0022-3727/18/12/004.

[37] G. Carson, A.J. Mulholland, A. Nordon, M. Tramontana, A. Gachagan, G. Hayward, Particle sizing using passive ultrasonic measurement of particle-wall impact vibrations, J. Sound Vib. 317 (2008) 142–157. https://doi.org/10.1016/j.jsv.2008.03.005.

[38] M. Guo, Y. Yan, Y. Hu, D. Sun, X. Qian, X. Han, On-line measurement of the size distribution of particles in a gas-solid two-phase flow through acoustic sensing and advanced signal analysis, Flow Meas. Instrum. 40 (2014) 169–177. https://doi.org/10.1016/j.flowmeasinst.2014.08.001.

[39] D.J. Buttle, S.R. Martin, C.B. Scruby, Particle Sizing by Quantitative Acoustic Emission, Res. Nondestruct. Eval. 3 (1991) 1–26. https://doi.org/10.1080/09349849109409499.

[40] T.B. Blank, S.D. Brown, Nonlinear Multivariate Mapping of Chemical Data Using Feed-Forward Neural Networks, Anal. Chem. 65 (1993) 3081–3089. https://doi.org/10.1021/ac00069a023.

[41] V. Prasad, B.W. Bequette, Nonlinear system identification and model reduction using artificial neural networks, Comput. Chem. Eng. 27 (2003) 1741–1754. https://doi.org/10.1016/S0098-1354(03)00137-6.

[42] M. Blanco, J. Coello, H. Iturriaga, S. Maspoch, J. Pagès, NIR calibration in non-linear

systems: Different PLS approaches and artificial neural networks, Chemom. Intell. Lab. Syst. 50 (2000) 75–82. https://doi.org/10.1016/S0169-7439(99)00048-9.

[43] V. Pauli, Y. Roggo, L. Pellegatti, N.Q. Nguyen Trung, F. Elbaz, S. Ensslin, P. Kleinebudde, M. Krumme, Process analytical technology for continuous manufacturing tableting processing: A case study, J. Pharm. Biomed. Anal. 162 (2019) 101–111. https://doi.org/10.1016/j.jpba.2018.09.016.

[44] M. Santl, I. ILIc, F. Vrecer, S. Baumgartner, A compressibility and compactibility study of real tableting mixtures: The effect of granule particle size, Acta Pharm. 62 (2012) 325–340. https://doi.org/10.2478/v10007-012-0028-8.

[45] M. Khorasani, J.M. Amigo, C.C. Sun, P. Bertelsen, J. Rantanen, Near-infrared chemical imaging (NIR-CI) as a process monitoring solution for a production line of roll compaction and tableting, Eur. J. Pharm. Biopharm. 93 (2015) 293–302. https://doi.org/10.1016/j.ejpb.2015.04.008.

FIGURES

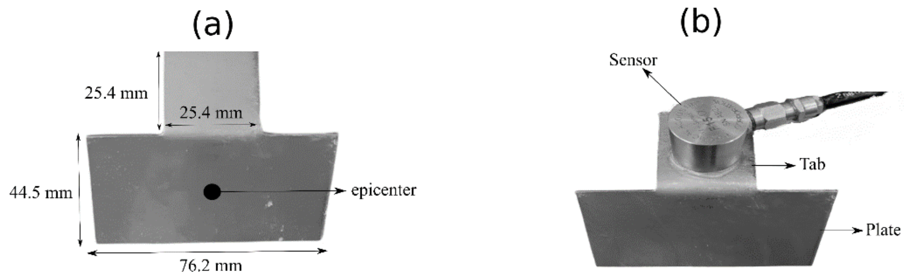

Figure 1. Top-down view of the impact plate inclined at 60 degrees relative to the horizontal plane (a) without and (b) with the acoustic emission sensor.

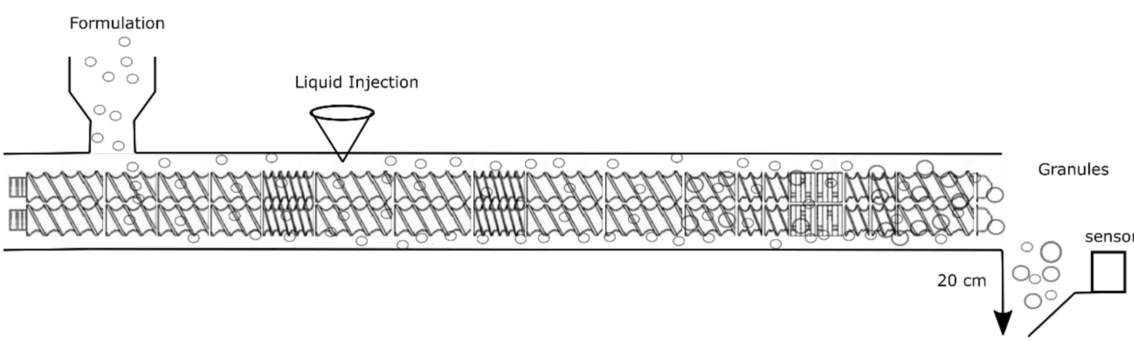

Figure 2. Schematic of the PAT setup for particle size monitoring, showing the twin-screw granulator and impact plate assembly positioned after its exit in the experiments.

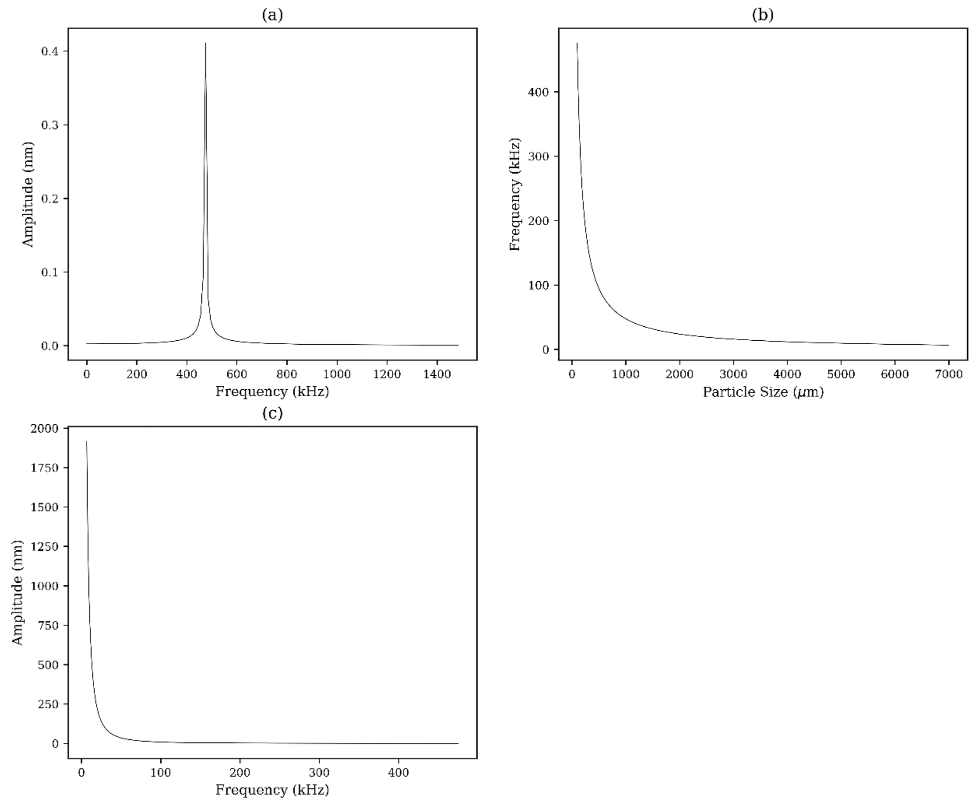

Figure 3. (a) Frequency spectrum for the plate response corresponding to a 100 μm particle collision. (b) Calculated frequencies corresponding to particles between 100 and 7150 μm particle collision with the plate at its epicenter. (c) Maximum amplitude and recorded frequency of particles between 100 and 7150 μm.

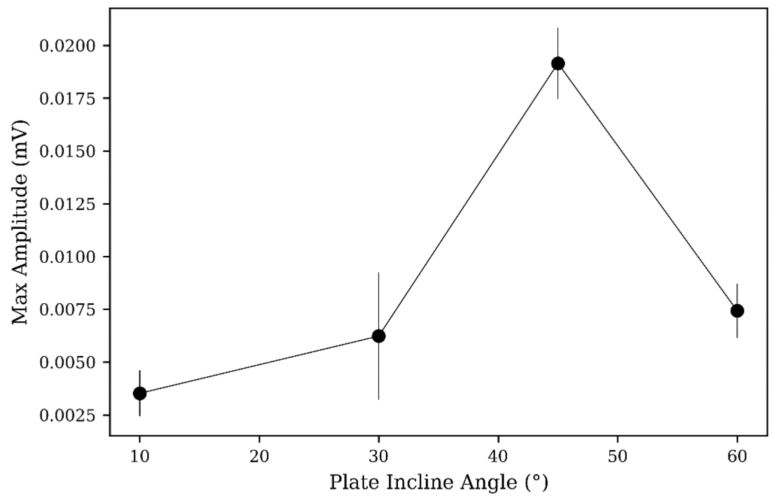

Figure 4. Average maximum amplitude of the AE spectra corresponding to changing incline plate angle.

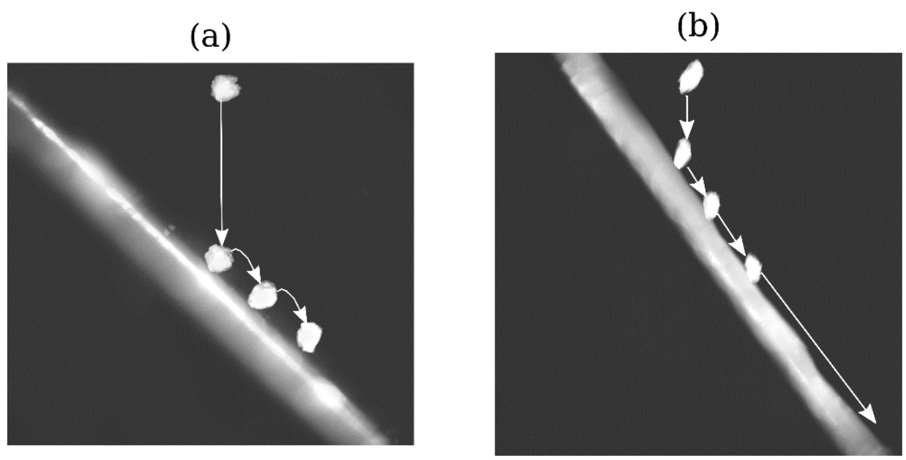

Figure 5. Trajectory of a particle on the impact plate with (a) 45 and (b) 60 degrees angle relative to the horizontal plate shown by super-imposing images over time. Arrows were shown to highlight the observed particle path followed.

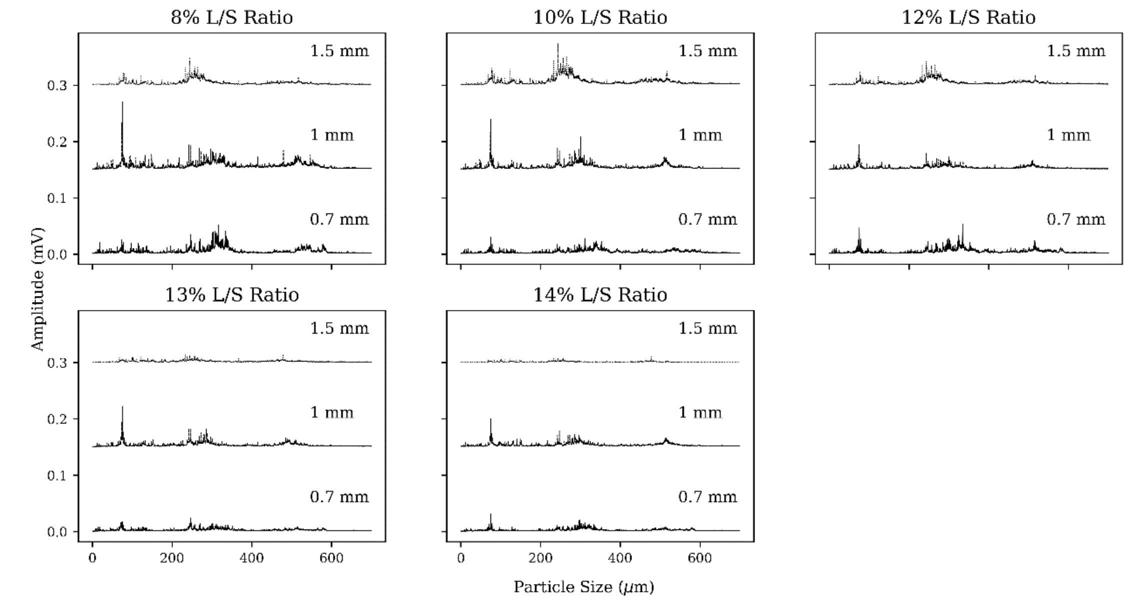

Figure 6. AE spectra for each L/S ratio for the impact plate inclined at 60 degrees for thicknesses of 0.7, 1, and 1.5 mm.

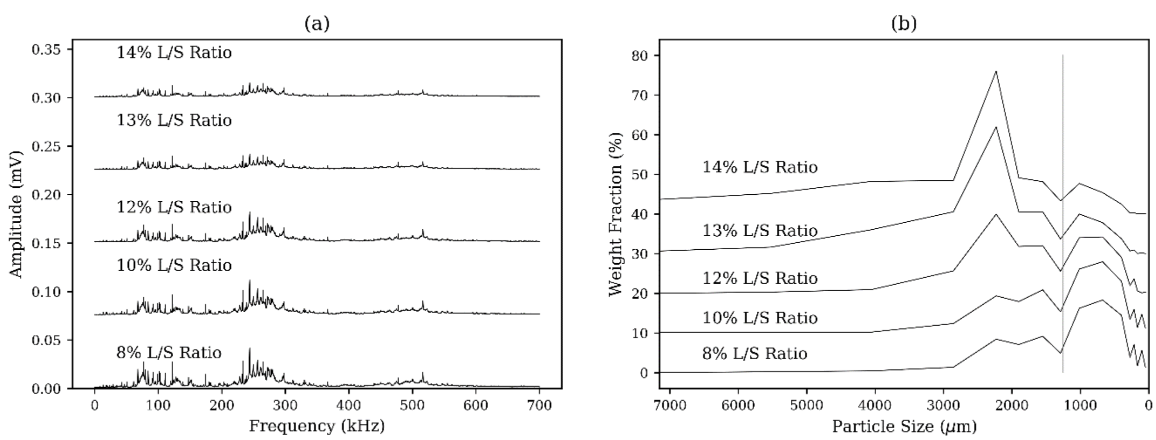

Figure 7. (a) Acoustic spectra of particle impacts for each L/S ratio. (b) PSDs for each L/S ratio. The vertical line indicates the often considered ideal size (1250 μm) suitable for tableting.

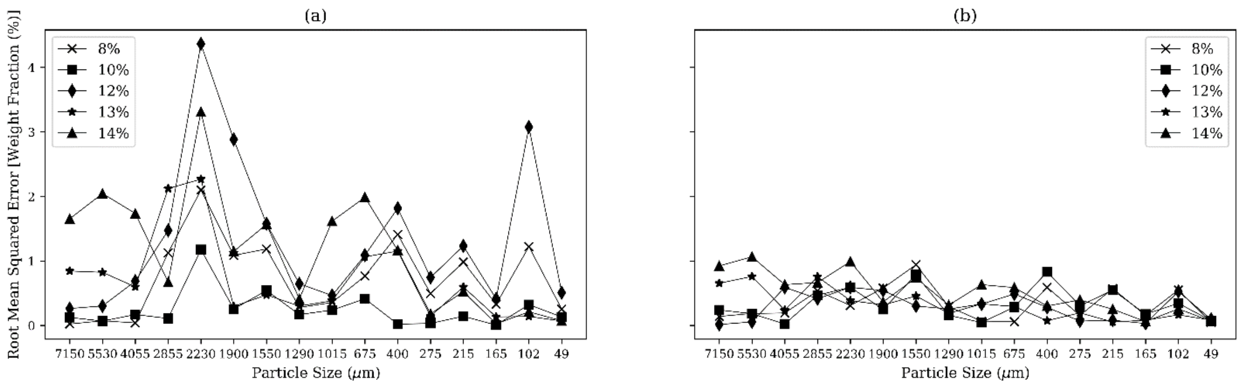

Figure 8. RMSE for every particle size at different L/S ratios for AE data (a) without and (b) with the impact filter.

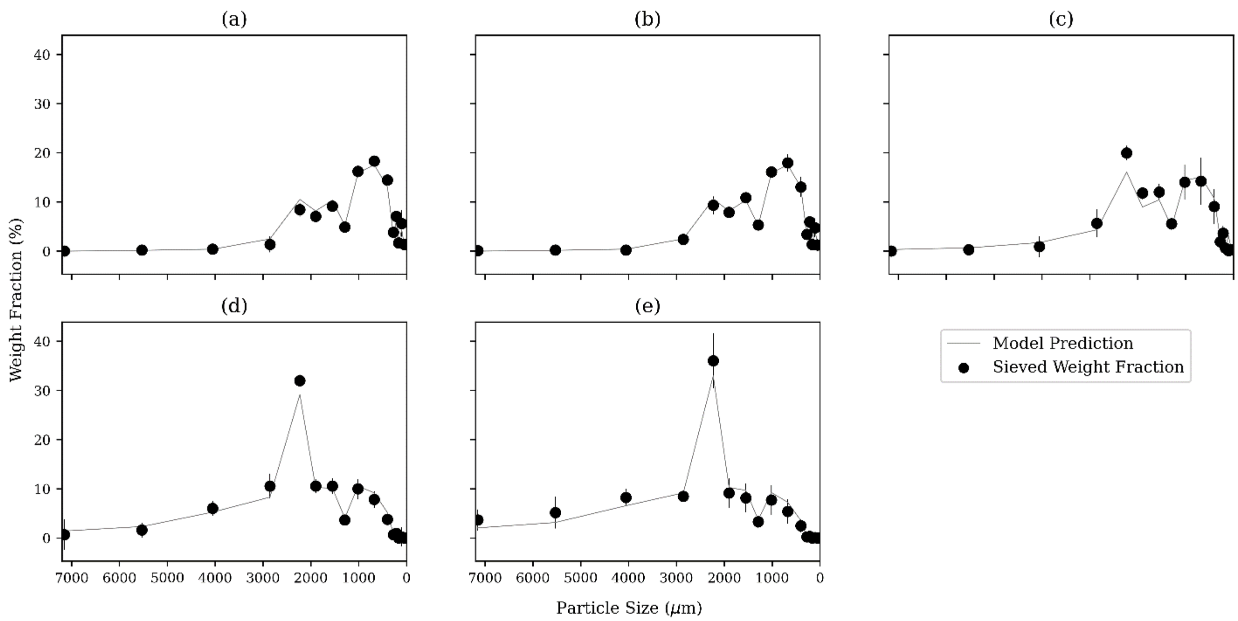

Figure 9. PSD predictions for (a) 8% (b) 10% (c) 12% (d) 13% and (d) 14% L/S ratio for AE spectral data without the impact filter. Error bars represent the standard deviation (n=3).

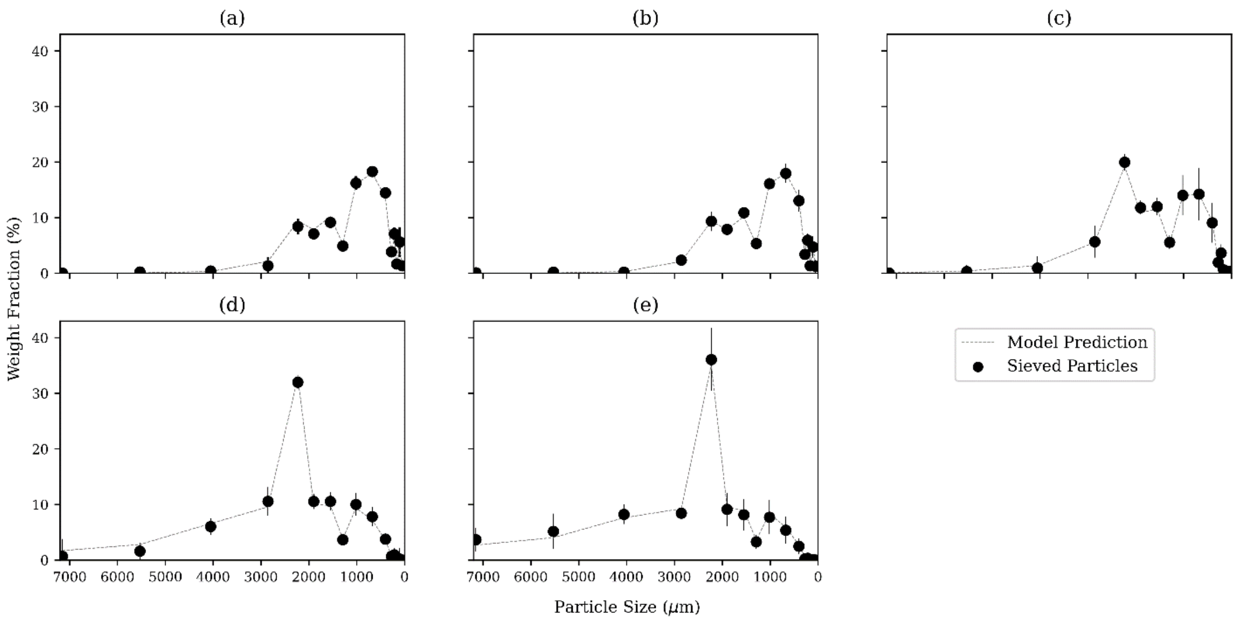

Figure 10. PSD predictions for (a) 8% (b) 10% (c) 12% (d) 13% and (d) 14% L/S ratio for AE spectral data with the impact filter. Error bars represent the standard deviation (n=3).